Optical Properties of Yb^{3+} and Nd^{3+}-Yb^{3+} Energy Transfer in $YAlO_3$†

M. J. Weber
Raytheon Research Division, Waltham, Massachusetts 02154
(Received 2 June 1971)

The optical absorption and emission spectra, $4f$ energy levels, fluorescence lifetime, and quantum efficiency of Yb^{3+} ions in $YAlO_3$ are reported. Fluorescence kinetics and $Nd^{3+} \rightarrow Yb^{3+}$ energy transfer were studied as a function of temperature in crystals codoped with Yb^{3+} and Nd^{3+}. Back transfer from Yb^{3+} to Nd^{3+} becomes important for Yb^{3+} relaxation at temperatures $\gtrsim 200$ °K. The rate and efficiency of $Nd^{3+} \rightarrow Yb^{3+}$ energy transfer in $YAlO_3$ are determined and compared with results for other materials. Stimulated-emission cross sections, $Cr^{3+} \rightarrow Nd^{3+} \rightarrow Yb^{3+}$ sensitization schemes, and possible Yb^{3+} laser action are also discussed.

INTRODUCTION

The optical spectrum of trivalent ytterbium arises from transitions between levels of the $^2F_{7/2}$ and $^2F_{5/2}$ manifolds of the $4f^{13}$ electronic configuration and is one of the simplest spectra of the lanthanide-series ions.[1,2] Transfer of electronic excitation between trivalent neodymium and trivalent ytterbium ions also provides a relatively simple case of nonradiative energy transfer between rare-earth ions.[3-6] The optical spectra of Yb^{3+} and $Nd^{3+} \rightarrow Yb^{3+}$ energy transfer have, therefore, been the subjects of numerous studies in both crystalline and glass hosts. Here these properties are reported in crystals of yttrium orthoaluminate. Since recent results have demonstrated that $YAlO_3$ is an excellent laser host crystal,[7-10] the stimulated-emission cross sections, sensitizing schemes, and possible laser action of Yb^{3+} in $YAlO_3$ are also investigated.

EXPERIMENT PROCEDURES

Large single crystals of $YAlO_3$ doped with Yb^{3+} and with Yb^{3+} plus Nd^{3+} were grown from stoichiometric melts by the Czochralski method[7] and annealed in a reducing atmosphere. The purity of the starting materials was 99.99%. The Yb content was established by spectrochemical analysis; quoted Yb concentrations are in atomic percent at Y sites. The distribution coefficient for Yb dopants in $YAlO_3$ is approximately unity.

Absorption and fluorescence spectra were recorded using a 0.5-m Jarrell-Ash grating monochromator equipped with a liquid-nitrogen-cooled S-1 photomultiplier. The samples were at room temperature or immersed in liquid nitrogen. A Cary Model 14 spectrophotometer was used for quantitative measurements of the absorption spectra.

For fluorescence kinetics studies, radiation from a combination of a xenon flashlamp with a 0.25-m grating monochromator was applied to pump ions into selected excited states; the resulting transient fluorescence signal was displayed on an oscilloscope and photographed. The temperature of the sample was varied by mounting it in a quartz Dewar through which flowed dry nitrogen gas. By a combination of a liquid-nitrogen heat exchange and a nichrome wire heater, the gas temperature was controlled from 77 to 700 °K. The sample temperature was measured with a thermocouple in contact with the crystal.

SPECTROSCOPIC PROPERTIES OF Yb^{3+}

Yttrium orthoaluminate has a distorted perovskite structure with four molecules in the orthorhombic unit cell (space group D_{2h}^{16}-$Pbnm$). Trivalent rare earths enter the lattice substitutionally at Y^{3+} sites which have C_{1h} point group symmetry. In this crystal-field symmetry, all but the Kramers degeneracy of the J manifolds is removed.

Examples of the $^2F_{5/2}$-$^2F_{7/2}$ absorption and fluorescence spectra of Yb^{3+} (2%) in $YAlO_3$ at 300 and 77 °K are shown in Figs. 1 and 2. Spectral lines were only partially polarized as expected for electric-dipole transitions in C_{1h} symmetry. Variations in relative line intensities with crystallographic orientation and polarization were not investigated in detail. In comparison to the $4f \rightarrow 4f$ spectra of other trivalent rare-earth ions in $YAlO_3$, the spectrum of Yb^{3+} is characterized (i) by broader linewidths, which increased with increasing temperature, and (ii) by the appearance of vibronic sidebands, which indicate stronger ion-lattice coupling.

The presence of vibronic transitions which rival some electronic transitions in intensity complicates the assignment of zero-phonon transitions and the determination of the energy-level scheme. A similar situation arose in the interpretation of the spectra of Yb^{3+} in yttrium gallium and aluminum garnets. To unravel the spectra, Buchanan *et al.*[2] carefully examined the vibronic sidebands in both absorption and in emission. Since for a given electronic transition these bands are expected to be

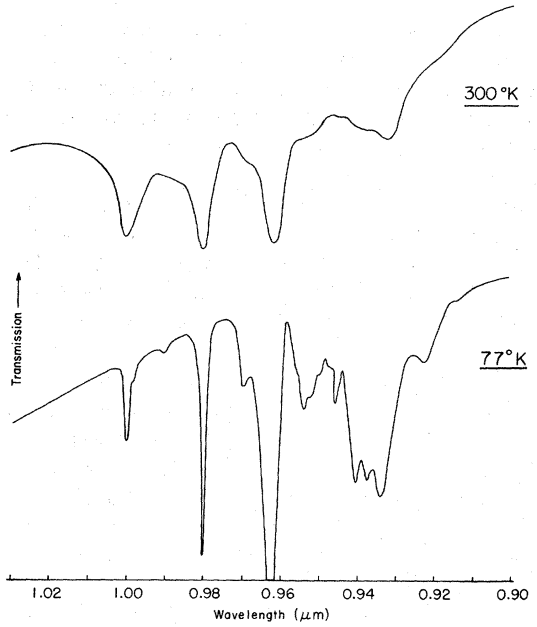

FIG. 1. $^2F_{7/2} \rightarrow {}^2F_{5/2}$ absorption spectrum of Yb^{3+} (2%) in $YAlO_3$; b axis, $E \perp c$.

approximately symmetric, any differences in the two bands were attributed to other electronic transitions. Interestingly, it was sufficient to consider only the vibronics associated with the transition between the lowest crystal-field levels of the $^2F_{7/2}$ and $^2F_{5/2}$ manifolds. This same approach was applied to the absorption and emission spectra of $YAlO_3 : Yb^{3+}$ at 300 and 77 °K to assign the electronic transitions; the resulting energy-level scheme is given in Fig. 3. The location of the highest-lying level of $^2F_{5/2}$ is least certain.

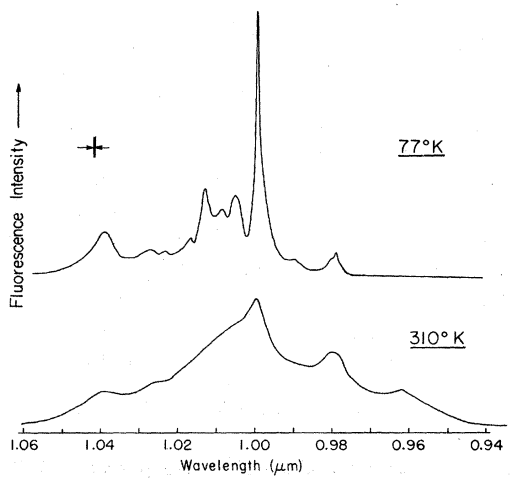

FIG. 2. $^2F_{5/2} \rightarrow {}^2F_{7/2}$ fluorescence spectrum of Yb^{3+} (2%) in $YAlO_3$; b axis, $E \perp c$.

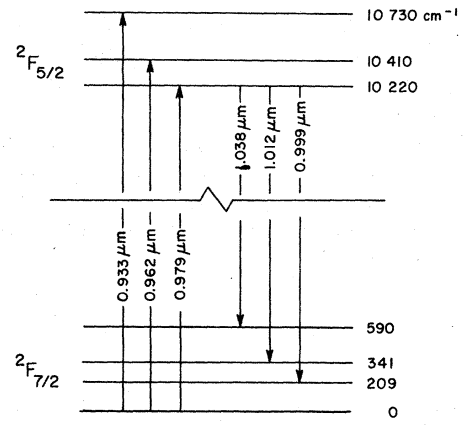

FIG. 3. Energy-level diagram and major transitions of Yb^{3+} in $YAlO_3$ at 77 °K.

Investigation of the electronic Raman scattering spectrum, as was done in the case of Yb^{3+} in the garnets,[11] would be useful in confirming these assignments.

The principal peaks of the Yb^{3+} vibronic spectrum are located at approximately 110, 280, 300, 430, and 500 cm^{-1} from the zero-phonon line. These frequencies exhibit general agreement with many peaks observed in the vibronic spectrum of Cr^{3+} in $YAlO_3$,[12] although the two ions occupy different lattice sites and hence the relative coupling to vibrational modes may be different.

The lifetime of the $^2F_{5/2}$ fluorescence was measured for sample temperatures ranging from 80 to 650 °K; the results are plotted in Fig. 4. Measurements were made using very small crystal samples to reduce the optical path length and thereby avoid radiation trapping.[13] The observed small decrease in lifetime with increasing temperature can arise from the increased probability for vibronic transitions, changes in the thermal

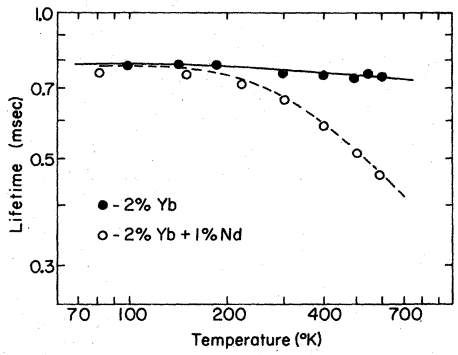

FIG. 4. Temperature dependence of the Yb^{3+} fluorescence lifetime in $YAlO_3$ doped with Yb and with Yb plus Nd. The dashed curve is the temperature dependence predicted from Eq. (9) using $\Delta = 700$ cm^{-1} and $\tau_{Nd} = 150$ μsec.

population distributions among the Stark levels of $^2F_{5/2}$ which have different decay probabilities, or the onset of nonradiative decay by multiphonon processes or energy migration.

To determine the radiative contribution to the $^2F_{5/2}$ lifetime and the quantum efficiency, the spontaneous emission probability A was found from measurements of the integrated absorption intensity via the relationship

$$A_{if} = \left(\frac{g_f}{g_i}\right) \frac{8\pi n^2}{N\lambda_0^2} \int k_{fi}(\nu)\, d\nu \,, \qquad (1)$$

where the g's are the degeneracies of the initial and final states, n is the refractive index, N is the number of Yb^{3+} ions per cm^3, $k(\nu)$ is the absorption coefficient at frequency ν, and λ_0 is the vacuum wavelength. Because the lines were broad and intense vibronic bands were present, no attempt was made to treat transitions between individual Stark levels of the $^2F_{5/2}$ and $^2F_{7/2}$ multiplets. Instead, the total room-temperature $^2F_{7/2} \rightarrow {}^2F_{5/2}$ absorption spectrum, including vibronics, was integrated using a planimeter, and the averaged intensity for the principal crystallographic directions of $YAlO_3$ together with an averaged wavelength of 1.0 μm were used in the above equation. N was measured by spectrochemical analysis. The resulting value of A was 1500 sec^{-1} corresponding to a radiative lifetine of 0.67 msec. This is less than the observed lifetime of 0.74 msec at 300 °K, presumably a result of the approximations made above. Therefore, within experimental uncertainties, the radiative quantum efficiency is unity. The absence of nonradiative processes is not unexpected because (i) nonradiative decay by multiphonon emission is very improbable due to the large $^2F_{5/2}$-$^2F_{7/2}$ energy gap and (ii) nonradiative decay by energy migration to quenching centers, if present, should be slow at Yb^{3+} concentrations of only 2%.

Nd^{3+}-Yb^{3+} ENERGY TRANSFER

Energy transfer between neodymium and ytterbium ions has been reported in several crystalline and glass hosts and attributed to pairs of transitions: Nd^{3+}-$^4F_{3/2} \rightarrow {}^4I_{9/2}$; Yb^{3+}-$^2F_{7/2} \rightarrow {}^2F_{5/2}$. The proximity and extent of the Nd^{3+} emission and Yb^{3+} absorption bands in $YAlO_3$ at 300 °K are shown in Fig. 5. Nd-Yb energy transfer was studied in $YAlO_3$: Yb (2%) crystals codoped with 1 and 3% Nd^{3+}. In these crystals the Nd^{3+} $^4F_{3/2} \rightarrow {}^4I_J$ fluorescence, while observable, was strongly quenched with respect to its intensity in Nd-only doped $YAlO_3$. That this arises predominantly from nonradiative energy transfer to Yb^{3+} was established from the fluorescence kinetics. Whereas in $YAlO_3$: Nd (1%) crystals the neodymium fluorescence decays exponentially with a lifetime of 150 μsec, in the $YAlO_3$: Yb (2%), Nd (1%) codoped crystals the neodymium decay was much faster and nonexponential. Examples of such decays are shown in Fig. 6. The nonexponential decay is a consequence of the various transfer rates for Nd-Yb pairs occupying different lattice sites and having different separations.

Nd^{3+}-to-Yb^{3+} energy transfer was confirmed by the presence of Nd^{3+} lines in the excitation spectrum of the Yb^{3+} fluorescence and by the time dependence of the Yb^{3+} fluorescence in pulsed selective excitation experiments. In the latter experiments, when Nd^{3+} ions were excited, the Yb^{3+} fluorescence intensity exhibited an initial transient buildup at a rate corresponding to excitation via transfer from excited Nd^{3+} ions. This is illustrated in Fig. 6. After the initial buildup, the Yb^{3+} fluorescence exhibited a simple exponential time dependence. The characteristic time for this decay for crystals containing 2% Yb^{3+} and 1% Nd^{3+} is plotted as a function of temperature in Fig. 4. The decrease in the Yb^{3+} lifetime of the Nd-codoped crystals is attributed to thermally activated back relaxation of Yb^{3+} via the faster relaxing Nd^{3+} ions.

Energy transfer between neighboring Nd^{3+} and Yb^{3+} ions must occur predominantly via pairs of transitions $^4F_{3/2} \rightarrow {}^4I_{9/2}$ (Nd^{3+}); $^2F_{7/2} \rightarrow {}^2F_{5/2}$ (Yb^{3+}). The energy mismatch for pairs of such transitions between individual Stark levels ranges from + 20 to + 1910 cm^{-1} which can be conserved by the creation of one or more phonons. The energy mismatch for $^4F_{3/2} \rightarrow {}^4I_{11/2}$ (Nd^{3+}); $^2F_{7/2} \rightarrow {}^2F_{5/2}$ (Yb^{3+}) transitions is of a similar magnitude but of opposite sign, hence phonon annihilation is required for energy conservation. Although the oscillator strengths of Nd^{3+} transitions from $^4F_{3/2}$ to $^4I_{11/2}$ are greater than to $^4I_{9/2}$,[14] energy transfer involving the former should be important only at very high temperatures.

Detailed treatment of the Nd^{3+}-Yb^{3+} energy transfer and its temperature dependence is complicated

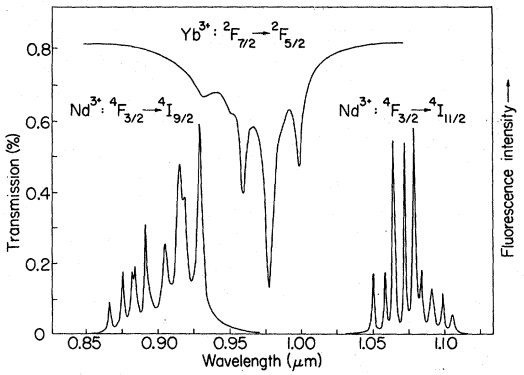

FIG. 5. Proximity of the Yb^{3+} absorption and Nd^{3+} fluorescence bands in $YAlO_3$ at 300 °K. The Nd^{3+} spectrum is uncorrected for the S-1 photocathode detection sensitivity. Absorption pathlength: 0.22 cm.

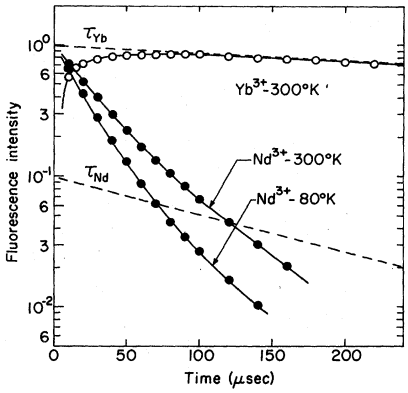

FIG. 6. Nonexponential decay of the Nd^{3+} fluorescence and the buildup of the Yb^{3+} fluorescence following pulsed excitation of Nd^{3+} in a $YAlO_3$ crystal codoped with Yb^{3+} (2%) and Nd^{3+} (1%). The dashed curves labeled τ_{Yb} and τ_{Nd} indicate the intrinsic decays of Yb^{3+} and Nd^{3+}.

by several factors: (a) There are several pairs of transitions with different oscillator strengths and energy mismatches; (b) for phonon-assisted transitions there are several ways of allocating phonons between the two ions; (c) changing thermal populations in the Stark manifolds alter the relative importance of the different transitions; and (d) the strength of the Nd^{3+}-Yb^{3+} coupling is strongly dependent upon the lattice sites of the two ions and is different for different pairings. Although by careful enumeration most of the above can be treated, in the past more gross approximations have been made to render the problem tractable. These include replacing the manifold of Stark levels by a single level and describing the net transfer probability by an effective rate constant R. Because of the uncertainties which arose in attempting to resolve the intensities of individual $^2F_{5/2} \rightleftharpoons {}^2F_{7/2}$ transitions for Yb^{3+}:$YAlO_3$, similar approximations are made below.

The essential features of the kinetics of the Nd^{3+}-Yb^{3+} energy transfer can be illustrated by considering the simplified energy-level system depicted in Fig. 7. τ_{Nd} and τ_{Yb} are the intrinsic lifetimes of excited Nd^{3+} and Yb^{3+} ions and w is the transfer probability coefficient for Nd^{3+} $^4F_{3/2} \rightarrow {}^4I_{9/2}$ and Yb^{3+} $^2F_{7/2} \rightarrow {}^2F_{5/2}$ energy exchange (a prime will denote the reverse process). Since Nd^{3+} ions excited into high-lying levels decay very rapidly (< 3 μsec) to $^4F_{3/2}$,[14] these levels are represented by a single pump band. If P is the optical pumping rate for Nd^{3+}, then the rate equations governing the level populations n in Fig. 7 are, neglecting radiative transfer,

$$\dot{n}_{Nd1} = -Pn_{Nd1} + \tau_{Nd}^{-1} n_{Nd2} + wn_{Nd2} n_{Yb1} - w' n_{Nd1} n_{Yb2} = -\dot{n}_{Nd2} ,$$

$$\dot{n}_{Yb1} = \tau_{Yb}^{-1} n_{Yb2} + w' n_{Nd1} n_{Yb2} - wn_{Nd2} n_{Yb1} = -\dot{n}_{Yb2} . \quad (2)$$

In the limit of weak pumping, where $n_{Yb1} \approx N_{Yb}$, $n_{Nd1} \approx N_{Nd}$, the solutions of these equations are of the form

$$n(t) = Ae^{-t/\tau_a} + Be^{-t/\tau_b} , \quad (3)$$

where

$$\frac{2}{\tau_{a,b}} = \frac{1}{\tau_{Nd}} + \frac{1}{\tau_{Yb}} + R + R' \pm \left[\left(\frac{1}{\tau_{Nd}} - \frac{1}{\tau_{Yb}} + R - R'\right)^2 + 4RR'\right]^{1/2} , \quad (4)$$

and the coefficients A and B are determined by the initial conditions at $t = 0$. The effective transfer rates are given by $R \approx wN_{Yb}$ and $R' \approx w'N_{Nd}$. If $R \gg R'$, the two exponents in Eq. (3) become $1/\tau_a = 1/\tau_{Nd} + R$ and $1/\tau_b = 1/\tau_{Yb}$. Thus following pulsed excitation of the Nd^{3+} system it exhibits a double exponential decay with an initial rate $1/\tau_a$ and a final rate $1/\tau_{Yb}$. Under the same conditions the Yb^{3+} system exhibits a transient behavior consisting of the difference of the same two exponential terms. These time dependences are reflected in the observed fluorescence responses shown in Fig. 6. The actual decays are more complex, however, because the effective R's are different from different Nd^{3+}-Yb^{3+} pairs. The observed macroscopic signal is an average over the entire ensemble of ion pairs in the sample; in the most general case this gives rise to nonexponential decays.[15]

The rate R and the quantum efficiency η of Nd^{3+}-to-Yb^{3+} energy transfer have, in previous studies,[3,5,6] been estimated simply from

$$R = \frac{1}{\tau} - \frac{1}{\tau_{Nd}} \quad (5)$$

and

$$\eta = 1 - \frac{\tau}{\tau_{Nd}} , \quad (6)$$

where τ is the lifetime of Nd^{3+} in the presence of Yb^{3+} and τ_{Nd} is the intrinsic lifetime of Nd^{3+}. If τ is defined as the time at which the fluorescence has decayed to e^{-1} of its initial value, then for $YAlO_3$:Yb(2%), Nd(1%) $\tau \approx 32$ μ sec at 300 °K (because of the finite duration of the excitation pulse used, ≈5 μsec, there is a small uncertainty in extrapolating the fluorescence intensity to its value at $t = 0$). The Nd^{3+} lifetime is concentration dependent[7]; at 1.0% Nd, the lifetime is 150 μsec. Using these values in Eqs. (5) and (6) yields $R = 2.5 \times 10^4$ sec^{-1} and $\eta = 0.79$. These values can be compared with those reported for $Na_{0.5}Gd_{0.46}Yb_{0.02}Nd_{0.02}WO_4$, where $R = 9 \times 10^3$ sec^{-1} and $\eta = 0.58$[3]; for $Ba_2MgGe_2O_7$ with

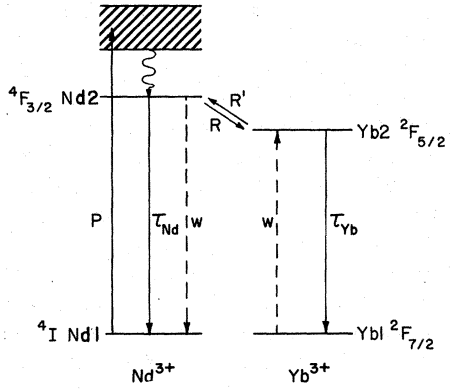

FIG. 7. Simplified energy-level schemes and transitions for the Nd^{3+}-Yb^{3+} system.

approximately 2-wt% Yb and Nd, where $R=7\times10^2$ sec^{-1} and $\eta=0.2$[5]; and for $LiYF_4$ with 2% YbF_3 and 2% NdF_3 in the initial melt, where $R=2.8\times10^3$ sec^{-1} and $\eta=0.58$.[6] Because of differences in the crystal structures and uncertainties in the actual Nd^{3+} and Yb^{3+} concentrations, direct quantitative comparison of these values is not possible. Nevertheless, semiquantitatively, the rate and efficiency of the $Nd^{3+}\rightarrow Yb^{3+}$ transfer in $YAlO_3$ appear to be high. At dopant levels of 2% Yb–1% Nd, each Nd^{3+} ion has, on the average, an Yb^{3+} ion within a sphere of radius ~8.5 Å, hence relatively strong multipolar coupling is possible.

The effective Nd-Yb coupling can change with temperature because of changes in the population distribution among the Stark levels and in the spectral profiles of the Nd^{3+} emission and Yb^{3+} absorption bands. The initial rate of Nd^{3+} decay at 77 °K is faster than at 300 °K (see Fig. 6). Using the measured τ of 24 μsec at 77 °K, $R=3.5\times10^4$ sec^{-1} and $\eta=0.84$.

The Nd^{3+} decay in the presence of Yb^{3+} is nonexponential, therefore the characteristic decay rate changes with time. The initial fast portion of the decay, which arises from Nd^{3+}-Yb^{3+} pairs having small separations, is weighted heavily in the e^{-1} definition of τ used in Eqs. (5) and (6). A more representative measure of the over-all transfer rate is obtained by defining a mean lifetime for the Nd^{3+} fluorescence given by

$$\tau_m=\int_0^\infty t\phi(t)\,dt\Big/\int_0^\infty \phi(t)\,dt\,, \tag{7}$$

where $\phi(t)$ is the transient fluorescence signal following an excitation pulse at time $t=0$. The corresponding expression for the quantum efficiency is

$$\eta=1-\frac{1}{\tau_0}\int_0^\infty \phi(t)\,dt\,. \tag{8}$$

For the 2% Yb, 1% Nd crystals, the mean Nd^{3+} lifetime, from Eq. (7), is ≈40 μsec at 300 °K. Using $\tau_m=\tau$ in Eq. (5) yields $R\approx1.8\times10^4$ sec^{-1}. From Eq. (8), $\eta\approx0.7$.

As shown in Fig. 4, when neodymium is present, the Yb^{3+} lifetime decreases with increasing temperature. At concentrations where $R\gg1/\tau_{Nd}$, $1/\tau_{Yb}$, the excited Nd^{3+} and Yb^{3+} systems rapidly come into thermal equilibrium; the Yb^{3+} system can then relax via back transfer to the faster relaxing Nd^{3+} ions. The decay rate in this limit is given by

$$\frac{1}{\tau}=\frac{1/\tau_{Yb}+(1/\tau_{Nd})(N_{Nd}/N_{Yb})\,e^{-\Delta/kT}}{1+e^{-\Delta/kT}(N_{Nd}/N_{Yb})}\,, \tag{9}$$

where Δ is the energy separation between the Nd2 and Yb2 levels in Fig. 7. The experimental data in Fig. 4 can be fitted by the dashed curve obtained using τ_{Yb} for the 2% Yb-only sample, $\tau_{Nd}=150$ μsec, and $\Delta=700$ cm^{-1} in Eq. (9). Although, because only a single transfer rate and energy difference Δ are considered, the quantitative values are only effective averages, the importance of back transfer in the $YAlO_3$:Yb, Nd system is established.

STIMULATED EMISSION

Stimulated emission involving $^2F_{5/2}\rightarrow{}^2F_{7/2}$ transitions of Yb^{3+} has been reported in glasses[16,17] and in two crystalline hosts, $Y_3Al_5O_{12}$[18] and CaF_2,[19] the latter sensitized with Nd^{3+}. Two promising transitions for obtaining laser action in $YAlO_3$:Yb^{3+} are the narrow intense line at 0.999 μm and the line at 1.038 μm which terminates on the highest-lying least-populated level of the $^2F_{7/2}$ manifold. The stimulated-emission cross sections for these lines were determined using two approaches. In the first, the cross section σ_{ij} for a transition of frequency ν between levels i and j was derived from the absorption spectrum and the relationship $\sigma_{ij}=\ln(I_0/I)_\nu/tN_i$, where N_i in the density of ions in the initial level i and t is the sample thickness. The largest cross section for the 0.999-μm line was observed in the crystallographic b direction and had a peak value of 2.1×10^{-20} cm^2 at 300 °K. A very weak 1.038-μm absorption was observed at 300 °K; the associated peak cross section was ~1.3×10^{-21} cm^2. This small value is in part a result of the large width of this line.

The cross sections at 77 °K were determined from the fluorescence spectrum and the branching ratios β_{ij}. Since the radiative quantum efficiency from the $^2F_{5/2}$ state is unity, the spontaneous emission probability for the line $i\rightarrow j$ at wavelength λ_{ij} is β_{ij}/τ, where τ is the $^2F_{5/2}$ lifetime. For a Lorentzian line, this is related to the cross section σ and linewidth $\Delta\nu$ by $\beta_{ij}/\tau=4\pi^2n^2\Delta\nu\sigma_{ij}/\lambda_{ij}$. Using this approach, peak b-axis cross sections of ≈1 $\times10^{-19}$ cm^2 and ≈6×10^{-21} cm^2 were found for the

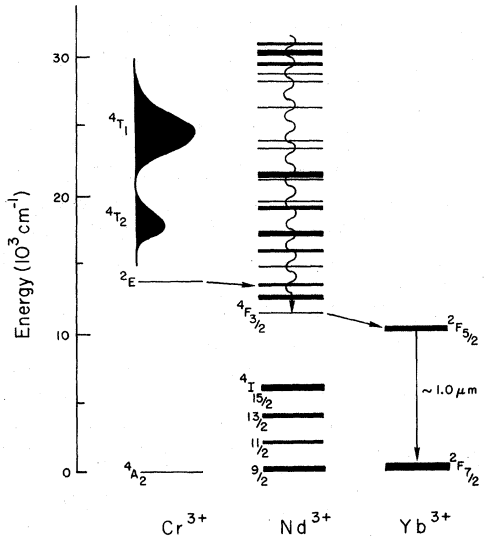

FIG. 8. Schematic diagram of the energy levels and energy transfer transitions for Cr^{3+}, Nd^{3+}, and Yb^{+3} in $YAlO_3$.

0.999- and 1.038-μm lines, respectively, of $YAlO_3$:Yb^{3+}(2%). These can be compared with a value of 1.25×10^{-19} cm^2 reported [20] for the most intense fluorescence line of $Y_3Al_5O_{12}$:Yb^{3+} at 77 °K.

At ambient temperatures the threshold for oscillation in $YAlO_3$:Yb^{3+} will be high because of the relatively small peak cross sections and because of the large thermal population in the terminal levels of the $^2F_{7/2}$ manifold. The latter can be reduced by lowering the crystal temperature; in addition, the lines narrow and the peak cross sections increase. In contrast to $Y_3Al_5O_{12}$:Yb^{3+}, where the most intense fluorescence line terminates on a high-lying, relatively unpopulated level of the $^2F_{7/2}$ manifold, in $YAlO_3$:Yb^{3+} the most intense line terminates on a level at only 209 cm^{-1} above the ground state. Even at 77 °K, the fractional ion population in this level is ≈0.02, thus only quasi-four-level laser operation should occur. For a crystal containing 1% ytterbium, 4×10^{18} excited Yb^{3+} ions per cm^3 would be required to achieve a threshold inversion.

Trivalent ytterbium has only one $4f$ absorption band for optical pumping, the $^2F_{5/2}$ manifold. This band, however, is well matched to the emission spectrum of GaAs:Si diodes. As demonstrated recently for $Y_3Al_5O_{12}$:Yb^{3+}, optical pumping by light emitting diodes can provide relatively efficient, low-heat-producing laser operation. [20]

To improve the optical pumping efficiency when other line or broad-band sources are used, trivalent neodymium can be added to sensitize the Yb^{3+} fluorescence because, as shown earlier, efficient $Nd^{3+}\rightarrow Yb^{3+}$ energy transfer occurs in $YAlO_3$ at concentrations $\gtrsim1\%$.

Since $Cr^{3+}\rightarrow Nd^{3+}$ energy transfer has been utilized in Nd^{3+} lasers, [9,21] the addition of trivalent chromium ions at Al^{3+} sites can further improve the pumping efficiency of Yb^{3+} via a series $Cr^{3+}\rightarrow Nd^{3+}\rightarrow Yb^{3+}$ process. This sensitization scheme is depicted schematically in Fig. 8. The combination of the broad $^4T_1$ and $^4T_2$ absorption bands of Cr^{3+} and the numerous absorption lines of Nd^{3+} (both of which are shown in Fig. 1 of Ref. 9) provides good utilization of visible and near-visible pump radiation.

To test the above sensitization scheme, the spectral properties of a $YAlO_3$ crystal containing 2% Yb, 1% Nd, and 0.1% Cr were examined. The fluorescence spectrum was identical to that observed for the $Yb^{3+}+Nd^{3+}$-doped crystals. The excitation spectrum of the Yb^{3+} fluorescence, however, showed the presence of both Nd^{3+} lines and the $^4T_1$ and $^4T_2$ bands of Cr^{3+} (the latter occur at 415 and 550 nm, respectively). The series energy transfer process $Cr^{3+}\rightarrow Nd^{3+}\rightarrow Yb^{3+}$ was confirmed by pulsed selective excitation experiments. The Yb^{3+} fluorescence, when excited by pumping into its own absorption band, exhibited a simple exponential decay. The Yb^{3+} fluorescence following excitation of Nd^{3+} consisted of an initial rapid buildup followed by a slow decay as described earlier. When pumping into the Cr^{3+} bands, however, the Yb^{3+} fluorescence exhibited an additional weak slow decay component. Since the intrinsic decay time of isolated Cr^{3+} ions in $YAlO_3$ is long (32 msec at 300 °K), this slow decay is attributed to transfer from excited Cr^{3+} ions. This transfer may occur either directly or via Nd^{3+} ions. The probability for direct transfer to Yb^{3+} is predicted to be small, however, because the rate of energy exchange between two ions depends exponentially upon the energy mismatch [22] and for pairs of Cr^{3+} $^2E\rightarrow{}^4A_2$; Yb^{3+} $^2F_{7/2}\rightarrow{}^2F_{5/2}$ transitions this energy difference is large, $\gtrsim3000$ cm^{-1}. In the case of transfer via Nd^{3+}, those excited Cr^{3+} ions near normal Nd^{3+} ions will transfer their excitation rapidly; the greater the Cr^{3+}-Nd^{3+} pair separation, however, the smaller the probability for transfer. Therefore the effective $Cr^{3+}\rightarrow Nd^{3+}\rightarrow Yb^{3+}$ transfer times will range from values limited by the $Nd^{3+}\rightarrow Yb^{3+}$ transfer time to values approaching the intrinsic Cr^{3+} decay time.

Any Yb^{3+} sensitizing scheme involving Nd^{3+} must contend with the possibility of stimulated emission of Nd^{3+} which can compete with $Nd^{3+}\rightarrow Yb^{3+}$ energy transfer. The peak cross sections for the principal $^4F_{3/2}\rightarrow{}^4I_{11/2}$ laser transitions of Nd^{3+} in $YAlO_3$ [14] are an order of magnitude larger than the $^2F_{5/2}\rightarrow{}^2F_{7/2}$ cross sections of Yb^{3+}. When Yb^{3+} is present, the $^4F_{3/2}$ lifetime and quantum efficiency are reduced due to nonradiative energy transfer to Yb^{3+}. Although this limits the excited Nd^{3+} population

buildup in the $^4F_{3/2}$ level, it is the inversion relative to a $^4I_{11/2}$ terminal level versus the Yb^{3+} $^2F_{5/2}$-$^2F_{7/2}$ inversion which governs the laser threshold. Since the former provides a four-level laser scheme at ambient temperatures whereas the latter provides only a quasi-four-level laser scheme even at 77 °K, stimulated emission from Nd^{3+} will normally have the lower threshold. Some frequency selective element would therefore be required in the optical resonator to introduce higher losses at the Nd^{3+} laser wavelengths and effectively discriminate against Nd^{3+} oscillation.

ACKNOWLEDGMENTS

The $YAlO_3$ crystals were grown by E. Comperchio and R. Monchamp. Their efforts and the experimental assistance of T. E. Varitimos throughout this investigation are very greatly appreciated.

†Research supported by the Night Vision Laboratory, Fort Belvoir, Va.

[1]G. H. Dieke, *Spectra and Energy Levels of Rare Earth Ions in Crystals* (Interscience, New York, 1968).

[2]R. A. Buchanan, K. A. Wickersheim, J. J. Pearson, and G. F. Hermann, Phys. Rev. 159, 245 (1967).

[3]G. E. Peterson and P. M. Bridenbaugh, J. Opt. Soc. Am. 54, 644 (1964); Appl. Phys. Letters 4, 201 (1964).

[4]T. F. Ewanisky, W. D. Grosse, and P. J. Caplan, J. Appl. Phys. 39, 2765 (1968).

[5]E. J. Sharp and J. E. Miller, J. Appl. Phys. 40, 4680 (1969).

[6]J. E. Miller and E. J. Sharp, J. Appl. Phys. 41, 4718 (1970).

[7]M. J. Weber, M. Bass, K. Andringa, R. R. Monchamp, and E. Comperchio, Appl. Phys. Letters 15, 342 (1969).

[8]G. A. Massey, Appl. Phys. Letters 17, 213 (1970).

[9]M. Bass and M. J. Weber, Appl. Phys. Letters 17, 395 (1970).

[10]G. A. Massey and J. M. Yarborough, Appl. Phys. Letters 18, 576 (1971).

[11]B. F. Argyle, R. L. Wadsack, and R. K. Chang, J. Appl. Phys. 42, 1478 (1971).

[12]M. J. Weber (unpublished).

[13]All samples available contained 2% Yb and radiation trapping was evident in crystals having dimensions >1 mm. In such samples the Yb^{3+} lifetime increased with increasing temperature as higher levels of the terminal $^2F_{7/2}$ manifold became thermally populated and the trapping probability increased.

[14]M. J. Weber and T. E. Varitimos, J. Appl. Phys. (to be published).

[15]M. J. Weber, this issue, Phys. Rev. B 4, 2932 (1971)

[16]E. Snitzer and C. G. Young, in *Advances in Lasers*, edited by A. Levine (Dekker, New York, 1968), Vol. 2, p. 191.

[17]C. G. Young, Proc. IEEE 57, 1267 (1969).

[18]L. F. Johnson, J. E. Geusic, and L. G. Van Uitert, Appl. Phys. Letters 7, 127 (1965).

[19]M. Robinson and C. K. Asawa, J. Appl. Phys. 38, 4495 (1967).

[20]A. R. Reinberg, L. A. Riseberg, R. M. Brown, R. W. Wacker, and W. C. Holton, Appl. Phys. Letters 19, 11 (1971).

[21]Z. J. Kiss and R. C. Duncan, Appl. Phys. Letters, 5, 200 (1964).

[22]T. Miyakawa and D. L. Dexter, Phys. Rev. B 1, 2961 (1964).

PHYSICAL REVIEW B VOLUME 4, NUMBER 9 1 NOVEMBER 1971

Hyperfine Magnetic Fields at Fe^{57} Nuclei in Ferrimagnetic Spinels*

F. van der Woude and G. A. Sawatzky†

Solid State Physics Laboratory, University of Groningen, Groningen, The Netherlands

(Received 11 February 1971)

The dependence of hyperfine fields at 0 °K at Fe^{57} nuclei in octahedral (*B*) and tetrahedral (*A*) sites in ferrites on the kind of nearest neighbors is discussed in terms of supertransferred hyperfine fields $H_{S\,THF}$. An expression for $H_{S\,THF}$ involving the various covalency parameters is derived using the linear combination-of-atomic-orbitals (LCAO) method. From experimental results and the derived expression for $H_{S\,THF}$, the various covalency parameters are determined for Fe^{3+} ions in both *A* and *B* sites. It is found that the $Fe^{3+}(A)$-O^{2-} bond is considerably more covalent than the $Fe^{3+}(B)$-O^{2-} bond and that the transfer of O^{2-} 2*p* electrons into Fe^{3+} 4*s* orbitals is proportional to the transfer into Fe^{3+} 3*d* orbitals. We have also found that the hyperfine fields in the various ferrimagnetic spinels can be explained to a large extent by considering only the changes in $H_{S\,THF}$.

The interesting magnetic properties of ferrimagnetic spinels and garnets originate mainly from the magnetic interactions between cations with magnetic moments which are situated in tetrahedral (*A*) and octahedral (*B*) sites. The hyperfine fields at Fe^{57} nuclei in *A* and *B* sites differ sufficiently for a detailed study with the Mössbauer-effect technique. As we have shown recently,[1] *B*-site nuclei with dif-